Inorganic Chemistry

Article

pubs.acs.org/IC

Four-Coordinate Iron(II) Diaryl Compounds with Monodentate *N*-Heterocyclic Carbene Ligation: Synthesis, Characterization, and Their Tetrahedral-Square Planar Isomerization in Solution

Yuesheng Liu,[†,§] Lun Luo,[‡,§] Jie Xiao,[†] Lei Wang,[†] You Song,[∥] Jingping Qu,[‡] Yi Luo,*[,‡] and Liang Deng*[,†]

[†]State Key Laboratory of Organometallic Chemistry, Shanghai Institute of Organic Chemistry, Chinese Academy of Sciences, 345 Lingling Road, Shanghai, People's Republic of China, 200032

[‡]State Key Laboratory of Fine Chemicals, School of Pharmaceutical Science and Technology, Dalian University of Technology, Dalian, People's Republic of China, 116024

[∥]State Key Laboratory of Coordination Chemistry, School of Chemistry and Chemical Engineering, Nanjing University, Nanjing, People's Republic of China, 210093

Supporting Information

ABSTRACT: The salt elimination reactions of $(IPr_2Me_2)_2FeCl_2$ (IPr_2Me_2 = 1,3-diisopropyl-4,5-dimethylimidazol-2-ylidene) with the corresponding aryl Grignard reagents afford $[(IPr_2Me_2)_2FeAr_2]$ (Ar = Ph, **3**; C_6H_4-*p*-Me, **4**; C_6H_4-*p*-^{t}Bu, **5**; C_6H_3-3,5-$(CF_3)_2$, **6**) in good yields. X-ray crystallographic studies revealed the presence of both tetrahedral and trans square planar isomers for **3** and **6** and the tetrahedral structures for **4** and **5**. Magnetic susceptibility and ^{57}Fe Mössbauer spectrum measurements on the solid samples indicated the high-spin (S = 2) and intermediate-spin (S = 1) nature of the tetrahedral and square planar structures, respectively. Solution property studies, including solution magnetic susceptibility measurement, variable-temperature ^{1}H and ^{19}F NMR, and absorption spectroscopy, on **3**–**6**, as well as an ^{57}Fe Mössbauer spectrum study on a frozen tetrahydrofuran solution of tetrahedral $[(IPr_2Me_2)_2{}^{57}FePh_2]$ suggest the coexistence of tetrahedral and trans square planar structures in solution phase. Density functional theory calculations on $(IPr_2Me_2)_2FePh_2$ disclosed that the tetrahedral and trans square planar isomers are close in energy and that the geometry isomerization can occur by spin-change-coupled geometric transformation on four-coordinate iron(II) center.

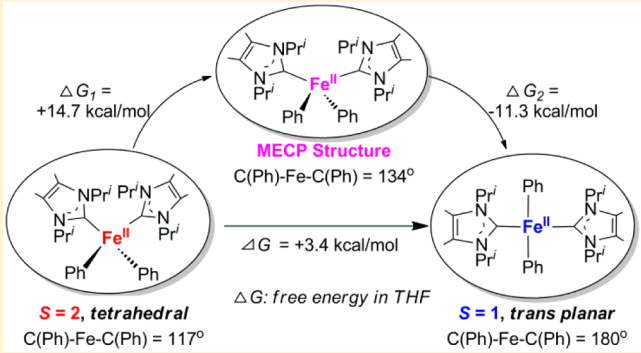

INTRODUCTION

Coordinatively unsaturated iron aryl species are commonly proposed intermediates in iron-catalyzed organic transformations[1−4] and have intrigued explorations on their exact nature. Studies have shown that this type of complex is usually highly reactive partially due to their open-shell nature[5] and can undergo reductive decomposition. For these reasons, the reactions of iron salts with PhLi and PhMgBr readily produce iron nanoparticles;[6] $[Fe(Mes)_2]_2$ is unstable at room temperature,[7] and the ferrate complex $[Li(Et_2O)_2][Li(1,4\text{-dioxane})][FePh_4]$ is prone to reductive decomposition at ambient conditions.[8] In contrast to these unstable binary iron(II) aryl complexes, plenty of four-, three-, and even two-coordinate iron aryl compounds with electron-withdrawing groups,[9] bulky substituents,[9b,10,11] or chelating donors[12] on the ortho positions of the aryl anions (A−F in Chart 1) are thermally robust. A handful of monophenyl iron(II) species with very bulky ancillary ligands are also scattering in literature (G−J in Chart 1).[13] While the studies on these "stabilized" iron aryl compounds have enriched our knowledge on the chemistry of open-shell organoiron species, the substituted aryl anions and the bulky ancillary ligands are not typical in iron catalysis, rendering the corresponding iron aryl compounds less catalytically relevant.

Noting the widely applied N-heterocyclic carbenes (NHCs) and phenyl metal reagents in iron-catalyzed organometallic transformations and their unravelled mechanism,[14] we initiated a project to pursue NHC-stabilized iron phenyl species. Our study showed that the use of a biphenyl-linked bis(benzimidazol-2-ylidene) ligand enables the preparation of high-spin tetrahedral iron(II) diaryl complexes [(bisNHC)$FeAr_2$] (Ar = Ph, **1**; C_6H_3-3,5-$(CF_3)_2$, **2** in Scheme 1a).[15] On the other hand, our attempts to prepare monodentate NHC-supported iron(II) phenyl complex $(NHC)_2FePh_2$ show that the selection of NHC ligand with appropriate steric bulkiness is

Received: January 21, 2015
Published: March 30, 2015

DOI: 10.1021/acs.inorgchem.5b00138
Inorg. Chem. 2015, 54, 4752−4760

Chart 1. Examples of Iron Aryl Complexes with Coordination Unsaturation

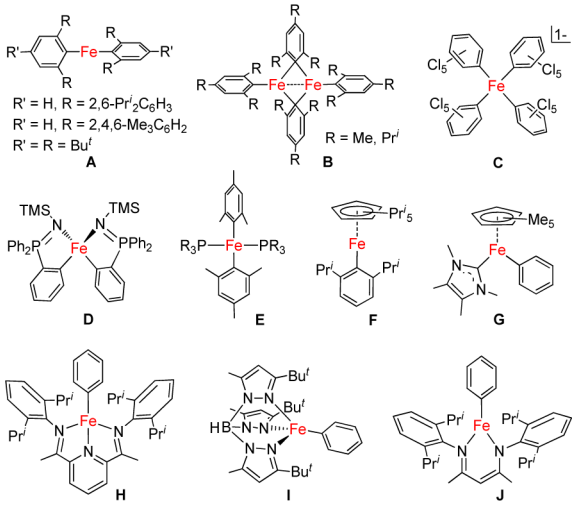

Scheme 1. Preparation of NHC−Iron(II)−Aryl Complexes

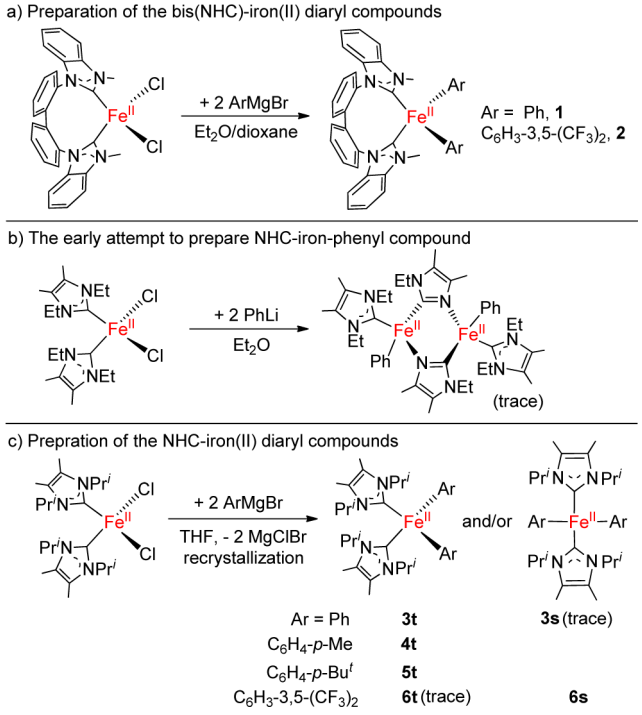

the key to achieve the stabilization of the desired iron(II) diphenyl compounds. We found that the reaction of $[(IPr)FeCl_2]_2$[16] (IPr = 1,3-di(2′,6′-diisopropylphenyl)imidazol-2-ylidene) with 2 equiv of PhMgBr produced iron black; the interaction of $(IEt_2Me_2)_2FeCl_2$ with 2 equiv of PhLi gave $[Ph(IEt_2Me_2)Fe(IEtMe_2)_2Fe(IEt_2Me_2)Ph]$ (IEt_2Me_2 = 1,3-diethyl-4,5-dimethylimidazol-2-ylidene, $IEtMe_2$ = 3-ethyl-4,5-dimethylimidazolyl anion; Scheme 1b);[17] the reaction of $(IPr_2Me_2)_2FeCl_2$ with PhMgBr, however, yielded a stable iron(II) diphenyl complex, tetrahedral $[(IPr_2Me_2)_2FePh_2]$ (**3t** in Scheme 1c).[18] Upon examining the reactions of the iron(II) diphenyl complex with alkyl halides, cyclooctatetraene, and ferrocenium cation, we further disclosed its reactivity of $C(sp^3)-C(sp^2)$ bond-formation cross-coupling, olefin coordination-induced biphenyl-reductive elimination, and one-electron oxidation-induced biphenyl-reductive elimination.[18]

In addition to the aforementioned findings, we also isolated a small amount of *trans*-$[(IPr_2Me_2)_2FePh_2]$ (**3s** in Scheme 1) from the reaction of $(IPr_2Me_2)_2FeCl_2$ with PhMgBr.[18] The attainment of the two isomers **3t** and **3s** raised a question as to whether they can form equilibrium in solution phase or not. This question could be important since the two isomers could have distinct ground spin states that might induce different reactivity.[5] Aiming to shed light on this problem, we report herein a systematic preparation and characterization study on the NHC−iron(II)−aryl complexes $[(IPr_2Me_2)_2FeAr_2]$ (Ar = Ph, C$_6$H$_4$-*p*-Me, C$_6$H$_4$-*p*-^{t}Bu, C$_6$H$_3$-3,5-(CF$_3$)$_2$). X-ray crystal structure determination, ^{57}Fe Mössbauer spectra, and magnetic susceptibility measurements on these iron(II) diphenyl species revealed that the iron(II) aryl complexes can exist as high-spin (S = 2) tetrahedral and/or intermediate-spin (S = 1) trans square planar isomers in solid states. Variable-temperature NMR, absorption spectra, solution magnetic moment measurements, solution ^{57}Fe Mössbauer spectrum, and theoretical studies collectively suggest that in solution phase a spin-change coupled geometry isomerization between tetrahedral and trans square planar structures can occur.

RESULTS AND DISCUSSION

Syntheses. The preparation of the monodentate NHC-coordinated iron(II) diaryl complexes employs the salt elimination reaction of $(IPr_2Me_2)_2FeCl_2$ with 2 equiv of the corresponding aryl Grignard reagents (Scheme 1c). After recrystallization, tetrahedral $[(IPr_2Me_2)_2FeAr_2]$ (Ar = C$_6$H$_4$-*p*-Me, **4t**; C$_6$H$_4$-*p*-^{t}Bu, **5t**) were obtained as yellow crystals in 50% and 53% isolated yields, respectively. Orange crystals of *trans*-$[(IPr_2Me_2)_2Fe(C_6H_3\text{-}3,5\text{-}(CF_3)_2)_2]\cdot 2$dioxane (**6s**·2C$_4H_8O_2$) were isolated as the major product in 52% yield along with a trace amount of tetrahedral $[(IPr_2Me_2)_2Fe(C_6H_3\text{-}3,5\text{-}(CF_3)_2)_2]$ (**6t**). The attempts to obtain **6t** in large quantity by recrystallization in different solvent and temperature were unsuccessful.

Solid-State Properties. The molecular structures of the diaryl compounds were established by single-crystal X-ray diffraction studies (Figure 1). Both tetrahedral and square planar structures were observed for **3** and **6**, and only the tetrahedral isomers were observed for **4** and **5** (Figure 1). ^{57}Fe Mössbauer and SQUID measurements corroborate a high-spin state (S = 2) for the tetrahedral isomers (**3t** and **5t**) and an intermediate-spin state (S = 1) for the trans square planar structure **6s**.

Table 1 compiles the key distances and angles around the FeC$_4$ cores for **4t**−**6s**, in addition with those of **1**−**3** for comparison. In the series of monodentate NHC-supported tetrahedral molecules (**3t**−**6t**), the Fe−C(aryl) distances being typical of the Fe−C(aryl) distances in high-spin iron(II) complexes (2.090(2), 2.119(2), 2.090(3), and 2.107(2) Å in average for **3t**−**6t**, respectively) are found to be independent of the electronic property of the substituents on the phenyl rings. The Fe−C(carbene) separations in **3t**−**6t** also span the narrow range from 2.137(2) to 2.162(2) Å and are close to those of the reported four-coordinate high-spin iron(II) NHC complexes.[17,19] Besides the similar bond distances, the range of the C−Fe−C angles and the relative orientation of the aryl and imidazole planes in **3t**−**6t** are different. These distinctions might be caused by crystal-packing force and the different steric properties of the aryl ligands. On the other hand, the

DOI: 10.1021/acs.inorgchem.5b00138
Inorg. Chem. 2015, 54, 4752−4760

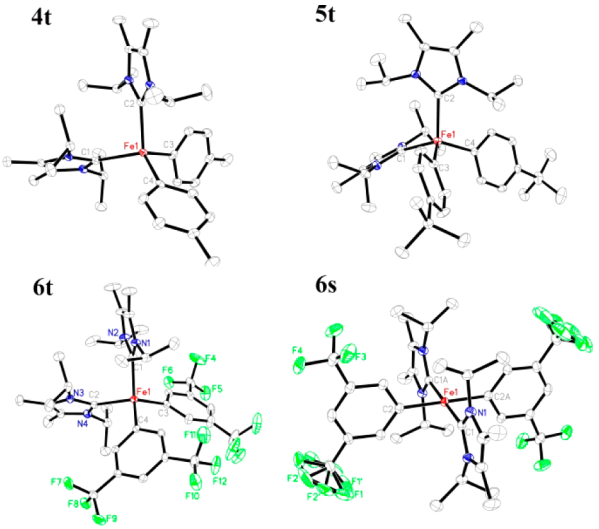

Figure 1. Molecular structures of **4t**, **5t**, **6t**, and **6s** showing 30% probability ellipsoids.

distinctions reflect the structural fluxionality of the FeC_4 tetrahedron. Two trans square planar structures (**3s** and **6s**) were observed in this series of diaryl complexes. The FeC_4 core in **6s** is essentially square planar, whereas that in **3s** shows a slight tetrahedral distortion (Table 1). The Fe−C(aryl) distances of the trans square planar compounds (2.032(4) and 2.003(4) Å in average for **3s** and **6s**, respectively) are close to those observed in *trans*-$[(PEt_2Ph)_2Fe(Mes)_2]$ (2.03 Å) and *trans*-$[(PEt_2Ph)_2Fe(C_6Cl_5)_2]$ (2.00 Å).[9b] Their Fe−C(carbene) distances (1.977(4) and 2.001(4) Å in average for **3s** and **6s**, respectively) are comparable to that in *trans*-$[(IMes)_2FeMe_2]$ (1.96 Å).[19e] The similarity points out their common intermediate-spin electronic configuration (S = 1). Consistent with this, the Fe−C(aryl) and Fe−C(carbene) distances in **3s** and **6s** are 0.06 and 0.19 Å, 0.10 and 0.14 Å shorter than those in their tetrahedral counterparts. Notably, in spite of the distinct geometries of the tetrahedral and square planar species, the metric data of their phenyl moieties are close to each other and typical of the aromatic rings.

Among the NHC-supported complexes, we measured the variable-temperature magnetic susceptibilities of **5t** and **6s** as the representative of tetrahedral and trans square planar structures. As shown in Figure 2, the magnetic susceptibilities of the solid sample of **5t** have μ_{eff} values ranging from 4.60 to 4.80 μB at 30−300 K. The data are comparable to the spin-only value of 4.90 μB for an S = 2 state. In the same temperature range, the measured magnetic moments of **6s** vary from 3.28 to 3.80 μB, which are larger than the spin-only value for an S = 1

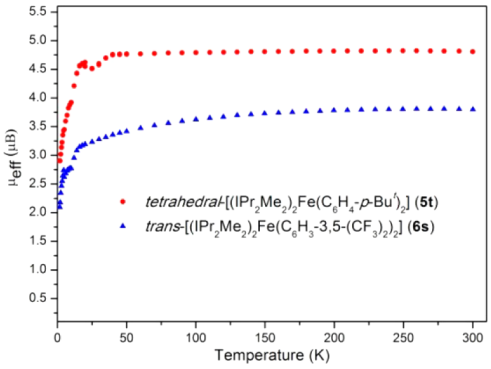

Figure 2. Temperature-dependent magnetic susceptibilities of **5t** (red) and **6s** (blue) in solid state.

state (2.83 μB) but still within the range of the reported intermediate-spin square planar iron(II) compounds. For examples, *trans*-$[(IMes)_2FeMe_2]$ has the magnetic moments of 2.7−3.2 μB (30−300 K);[19e] *cis*-$[(dppe)Fe(Mes)_2]$ has the data of 3.3−3.9 μB (50−300 K).[9b] The large magnetic moments of **6s** might be due to the presence of trace amounts of its high-spin tetrahedral isomer in the solid sample and/or the contributions of spin−orbit coupling in the planar structure as observed in Chirik's square planar cobalt complexes.[20]

The zero-field ^{57}Fe Mössbauer spectra of **3t**, **5t**, and **6s** further support the high-spin and intermediate-spin nature of tetrahedral and square planar structures, respectively. Supporting Information, Figures S1 and S2 show the spectra of **5t** and **6s**, respectively. Table 2 lists the fitting isomer shifts (δ) and quadrupole splittings (ΔE_Q). The data of **3t** (δ = 0.47 mm/s, ΔE_Q = 2.38 mm/s)[18] and **5t** (δ = 0.45 mm/s, ΔE_Q = 2.40 mm/s) are close to those of the tetrahedral iron(II) dialkyl complex $[(IEt_2Me_2)_2Fe(CH_2SiMe_3)_2]$ (δ = 0.49 mm/s, ΔE_Q = 2.53 mm/s, Supporting Information, Figure S3). The Mössbauer data of the trans square planar complex **6s** (δ = 0.17 mm/s, ΔE_Q = 4.09 mm/s) are comparable to those of the reported intermediate-spin square planar iron(II) species, for example, $[((^{i\text{-Pr}}C)_2Ph)_2Fe]I_2$ (δ = 0.18 mm/s, ΔE_Q = 4.16 mm/s) ($(^{i\text{-Pr}}C)_2Ph$ = *o*-bis(3-isopropyl-imidazol-2-ylidene)benzene),[19a] *trans*-$[(PEt_3)_2Fe(C_6Cl_5)_2]$ (δ = 0.27 mm/s, ΔE_Q = 4.16 mm/s),[21] *cis*-[(Sciopp)Fe(Mes)$_2$] (δ = 0.29 mm/s, ΔE_Q = 3.58 mm/s) (Sciopp = 1,2-bis(di(3′,5′-di(*t*-butyl)phenyl)phosphino)-benzene),[10j] and *trans*-$[(PEt_2Ph)_2Fe(Mes)_2]$ (δ = 0.31 mm/s, ΔE_Q = 4.63 mm/s).[9b] The lower isomer shift of **6s** as compared to those of the phosphine-coordinated complexes reflects the stronger σ-donating nature of the NHC ligand over the phosphines.[22]

Table 1. Selected Interatomic Distances (Å) and Angles (deg) of 1−6 from Crystal Structures

	1	2	3t	3s	4t	5t	6t	6s
Fe−C(aryl)	2.077(2)	2.073(3)	2.090(2)	2.014(4)	2.121(2)	2.080(3)	2.114(2)	2.003(4)
	2.070(2)	2.074(3)	2.091(2)	2.049(4)	2.117(2)	2.099(3)	2.101(2)	2.003(4)
Fe−C(carbene)	2.076(2)	2.110(2)	2.157(2)	1.973(4)	2.151(2)	2.146(3)	2.137(2)	2.001(4)
	2.095(2)	2.116(2)	2.162(2)	1.980(4)	2.152(2)	2.158(3)	2.149(2)	2.001(4)
α^a	108.4(1)	121.3(1)	114.0(1)	175.9(2)	99.5(1)	112.2(1)	100.1(1)	180
β^b	110.0(1)	116.6(1)	113.3(1)	176.6(2)	109.7(1)	115.1(1)	109.4(1)	180
γ^c	73.8	85.2	87.8		85.1	84.2	79.5	

[a] α = ∠C(aryl)−Fe−C(aryl). [b] β = ∠C(carbene)−Fe−C(carbene). [c] Dihedral angles between the planes C(carbene)−Fe−C(carbene) and C(aryl)−Fe−C(aryl).

DOI: 10.1021/acs.inorgchem.5b00138
Inorg. Chem. 2015, 54, 4752−4760

Table 2. ^{57}Fe Mössbauer Parameters for Iron(II) Aryl and NHC Complexes Recorded at 80 K

	δ (mm/s)	ΔE_Q (mm/s)	%
3t	0.47	2.38	100
5t	0.45	2.40	100
6s	0.17	4.09	100
$[(IEt_2Me_2)_2Fe(CH_2SiMe_3)_2]$	0.49	2.53	100
$[((^{i\text{-}Pr}C)_2Ph)_2Fe]I_2$[a]	0.18	4.16	100
trans-$[(PEt_3)_2Fe(C_6Cl_5)_2]$[b]	0.27	4.16	100
trans-$[(PEt_2Ph)_2Fe(Mes)_2]$[c]	0.31	4.63	100
cis-[(Sciopp)Fe(Mes)$_2$][d]	0.29	3.58	100
3t-^{57}Fe[e]	0.43	2.39	93
3t-^{57}Fe **in frozen THF**[f]	0.48	2.45	21
	0.22	4.15	71

[a]Reference 19a. [b]Reference 21; 79 K. [c]Reference 9b. [d]Reference 10j. [e]In addition to the major component corresponding to tetrahedral $[(IPr_2Me_2)_2{}^{57}FePh_2]$ (**3t**-^{57}**Fe**), a minor doublet (7% area) with δ = 0.59 mm/s, ΔE_Q = 2.85 mm/s, which might correspond to $[(IPr_2Me_2)_2{}^{57}FePhBr]$,[18] was noticed. [f]The minor doublet corresponding to $[(IPr_2Me_2)_2Fe^{57}PhBr]$[18] was also noticed.

Solution Properties. Compounds **3t**, **4t**, **5t**, and **6s** are quite soluble in common organic solvent, such as benzene, diethyl ether, and tetrahydrofuran (THF). In C_6D_6, the ^{1}H NMR spectra of these diphenyl compounds generally show two or three heavily broadened signals (+62 and −7 ppm for **3t**; +66, +63, and −1 ppm for **4t**; +62, +17, and −6 ppm for **5t**; −8 and −11 ppm for **6s**). The ^{1}H NMR spectra measured in THF-d_8 (for **3t**, **5t**, and **6s**) are close to those obtained in C_6D_6. Their measured solution magnetic moments in benzene are 4.2(2), 4.4(1), 4.1(2), and 4.4(2) μB for **3t**−**6s**, respectively.[23] These values are smaller than the spin-only value for a high-spin iron(II) species (4.90 μB) but larger than that of intermediate-spin iron(II) compounds (2.83 μB). Moreover, the value of **5t** is slightly lower than those of the SQUID data for the solid sample, whereas the solution data of **6s** is larger than that of its solid sample.

Dissolution of the diaryl complexes in benzene produces deep yellow solutions. Their absorption spectra recorded in benzene at room temperature all feature two near-infrared bands at ca. 1350 and 1500 nm for **3t**−**5t** and at 1320 and 1420 nm for **6s** (Figure 3). The numbers of the observed near-infrared absorption bands of **3**−**6** are different from those of reported tetrahedral and square planar iron(II) complexes. For example, the absorption spectra of the tetrahedral bis(NHC)−Fe(II)−diaryl complexes **1** and **2** exhibit one broad near-infrared band at 1330 and 1410 nm, respectively;[15] the spectrum of the square planar compound *trans*-[(IMes)$_2$FeMe$_2$][19e] shows three near-infrared bands at 900, 980, and 1415 nm (Figure 3); and *cis*-[(Sciopp)Fe(Mes)$_2$] has its three ligand-field transition bands centered at 1075, 1328, and 1575 nm.[10j] Moreover, the absorption coefficiencies of **3**−**6** are located between those of the strict tetrahedral complexes (**1** and **2**) that have relaxed LaPorte selection rule for ligand-field transitions and the strict planar complex (*trans*-[(IMes)$_2$FeMe$_2$]) that has the LaPorte-forbidden transition These differences, in addition with the unusual solution magnetic moments, hint that the monodentate NHC-coordinated iron(II) diaryl complexes may not exist solely as a tetrahedral or a trans square planar form in solution phase.

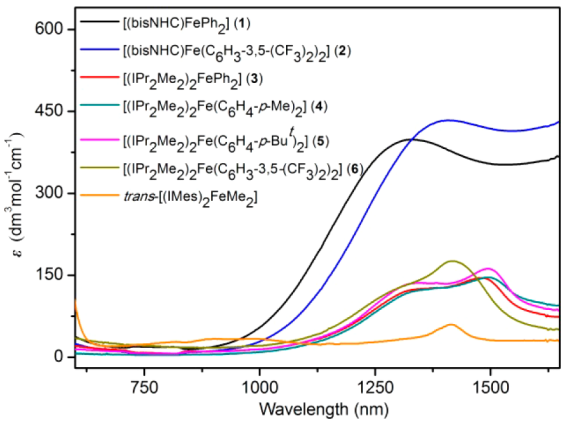

Figure 3. Absorption spectra of **1**−**6** and *trans*-[(IMes)$_2$FeMe$_2$] in the near-infrared region measured in benzene at room temperature.

We further performed variable-temperature NMR (VT-NMR) studies on the THF-d_8 solutions of these iron(II) diaryl complexes. As shown in Figure 4 and Supporting Information,

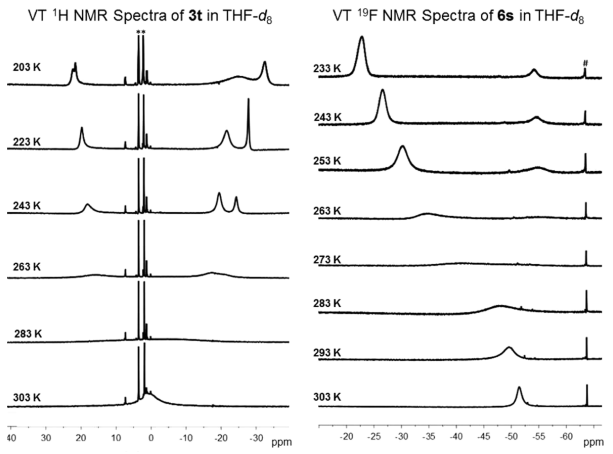

Figure 4. Variable-temperature ^{1}H NMR spectra of **3t** (left) and ^{19}F NMR spectra of **6s** (right) measured in THF-d_8. For simplicity, only the selected regions are shown. Signals marked (*) correspond to THF-d_8 and solvent residue, and the ones marked (#) correspond to 1,3-$(CF_3)_2$-C_6H_4.

Figures S5 and S6, the ^{1}H NMR spectra of **3t**, **5t**, and **6s** exhibit peak-decoalescing phenomena along with temperature-dependence of the isotropic shifts when lowering the temperature from 303 to 203 K. For example, at 243 K, the spectrum of **3t** displays three well-separated intense peaks at −24.4, −19.5, and +18.1 ppm. Decreasing the temperature to 203 K results in the splitting of the lower-field peak (the one at +18.1 ppm) into two (Figure 4). In addition to the VT-^{1}H NMR studies, the VT-^{19}F NMR spectra of the solution of **6s** also exhibit the decoalescing of one ^{19}F NMR singal at −52 ppm at 303 K into two peaks (−24 and −57 ppm) at 233 K (Figure 4). These peak-decoalescing phenomena could be due to restricted rotation of the aryl and NHC ligands at low temperature or the fluxional process of tetrahedral-to-square planar isomerization. The former speculation seems less likely as the VT-^{19}F NMR spectra of tetrahedral $[(bisNHC)Fe(C_6H_3\text{-}3,5\text{-}(CF_3)_2)_2]$ (**2**) only show one ^{19}F NMR signal in the temperature range from 303 to 233 K (Supporting Information, Figure S7).

The convincing evidence for the tetrahedral-to-square planar isomerization of the iron(II) diaryl complexes was obtained from the ^{57}Fe Mössbauer spectrum of a frozen THF solution of

DOI: 10.1021/acs.inorgchem.5b00138
Inorg. Chem. 2015, 54, 4752−4760

tetrahedral $[(IPr_2Me_2)_2{}^{57}FePh_2]$ (**3t-^{57}Fe**). The ^{57}Fe-enriched crystalline sample has its ^{57}Fe Mössbauer spectrum identical to that of **3t** (Figure 5a and Table 2). The Mössbauer spectrum of its frozen THF solution prepared by dissolving the crystalline sample into THF, however, shows two quadrupole doublets (Figure 5b) with the area ratio of 7:2 and the fitting parameters of δ = 0.22 mm/s, ΔE_Q = 4.15 mm/s for the major component and δ = 0.48 mm/s, ΔE_Q = 2.45 mm/s for the minor one. The parameters of the two components are apparently similar to those of the solid samples of **6s** and **5t**, respectively (Table 2), which suggest the frozen solution contains a mixture of intermediate-spin *trans*-$[(IPr_2Me_2)_2{}^{57}FePh_2]$ and high-spin tetrahedral $[(IPr_2Me_2)_2{}^{57}FePh_2]$, with the trans square planar isomer dominating. Noting the resemblance of the aforementioned solution properties of **3t** with those of **4t**–**6s**, we reason that in solution phase all these monodentate NHC-supported iron(II) diaryl species should present as mixtures of tetrahedral and trans square planar isomers.

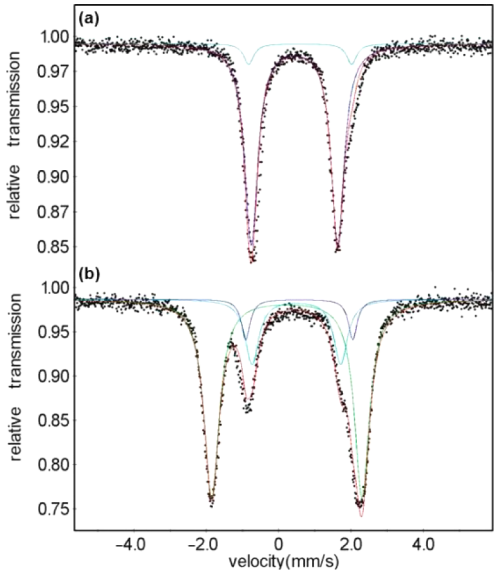

Figure 5. Zero-field ^{57}Fe Mössbauer spectra measured on (a) a polycrystalline solid of $[(IPr_2Me_2)_2{}^{57}FePh_2]$ (**3t-^{57}Fe**) and (b) a frozen THF solution of **3t-^{57}Fe** at 80 K. The color lines are the fitting curves. Fitting parameters are listed in Table 2. A minor doublet with the area percentage of ca. 7% was noticed in both spectra, which might correspond to trace amount of $[(IPr_2Me_2)_2{}^{57}FePhBr]$.

Isomerization Mechanism. As the characterization data suggest the presence of tetrahedral–square planar isomerization process in solution phase, we further performed density functional theory (DFT) calculations[24,25] to probe the possible mechanism. Geometry optimizations on $(IPr_2Me_2)_2FePh_2$ at S = 2 and S = 1 states proved that the energy minima at the two spin states have distorted tetrahedral and trans square planar geometries (**3t-opt** and **3s-opt**), respectively. Both the optimized structures nicely reproduced the key interatomic distances and angles (Table 3) observed in the crystal structures.

Molecular orbital analyses indicate that, in the case of **3t-opt**, its five highest occupied molecular orbitals (four singly occupied molecular orbitals and one doubly occupied molecular orbital, as shown in Figure 6) are mainly iron-based (atomic

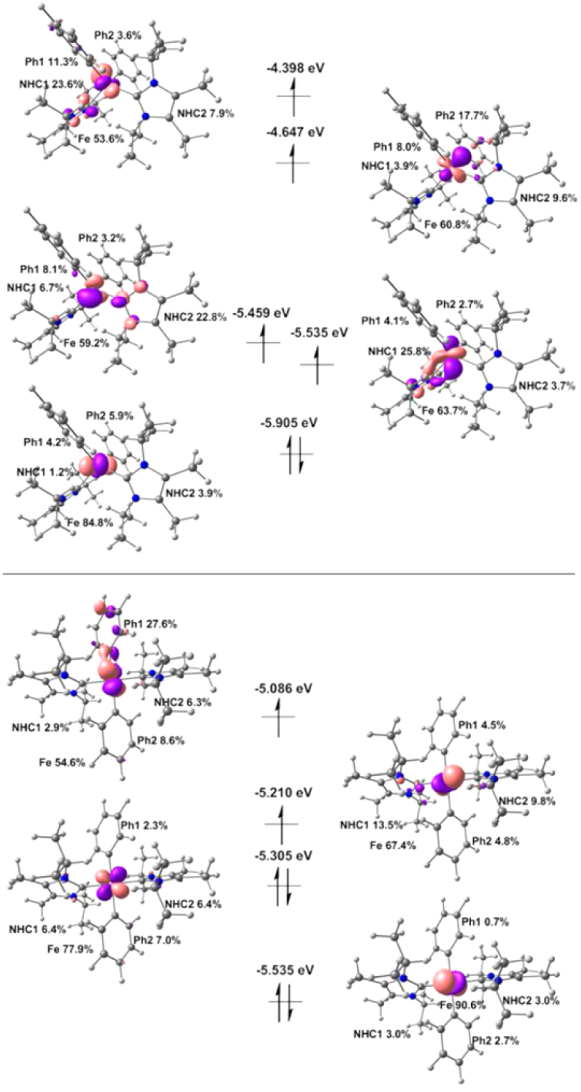

Figure 6. Schematic MO diagrams for UKS solutions (B3LYP/TZVP) of **3t-opt** (upper, S = 2) and **3s-opt** (lower, S = 1).

Table 3. Selected Bond Distances (Å) and Angles (deg) of 3t, 3t-opt, 3s, 3s-opt, and MECP2[a]

	3t	3t-opt	MECP2	3s-opt	3s
Fe–C(aryl)	2.090(2)	2.117	2.075	2.080	2.014(4)
	2.091(2)	2.123	2.064	2.081	2.049(4)
Fe–C(carbene)	2.157(2)	2.223	2.064	1.998	1.973(4)
	2.162(2)	2.228	2.192	1.998	1.980(4)
α[b]	114.0(1)	116.79	133.94	179.8	175.9(2)
β[c]	113.3(1)	112.96	140.33	179.5	176.6(2)

[a]**MECP2** denoted for the structure of the minimum energy crossing point of the S = 1 and S = 2 energy surfaces of $(IPr_2Me_2)_2FePh_2$. [b]α = ∠C(aryl)–Fe–C(aryl). [c]β = ∠C(carbene)–Fe–C(carbene).

DOI: 10.1021/acs.inorgchem.5b00138
Inorg. Chem. 2015, 54, 4752–4760

orbital contribution varying from 53.6% to 84.8%). Small orbital contribution from the NHC ligands having π^*-character is also noticeable, but the $3d_{Fe} \rightarrow \pi^*_{NHC}$ backdonation is insignificant because of the ineffective orbital overlapping. Thus, **3t-opt** is a typical high-spin iron(II) species. The Wiberg bond indexes of its Fe−C(aryl) and Fe−C(carbene) bonds are 0.53 and 0.50, respectively. The Mulliken spin-density analysis further suggests that the four spins reside primarily on the iron center (Supporting Information, Figure S8). In **3s-opt**, the Fe−C(aryl) and Fe−C(carbene) bonds have larger Wiberg bond indexes (0.62 and 0.67) and shorter bond distances (2.08 and 2.00 Å) in comparison with those in **3t-opt** (WBIs of 0.53 and 0.50, and distances of 2.12 and 2.22 Å), suggesting a stronger Fe−C bonding in **3s-opt**. The shorter Fe−C(carbene) distances, however, do not mean enhanced $3d_{Fe} \rightarrow \pi^*_{NHC}$ backdonation in **3s-opt** as weak π-type metal-to-ligand backdonation in **3s-opt** occurs on the phenyl fragments, rather than the NHCs (Figure 6). The orbital compositions of the four highest occupied frontier orbitals in combination with the spin-density distribution (Supporting Information, Figure S9) are suggestive of the intermediate-spin ferrous nature of **3s-opt**.

In spite of their distinct structures, it is worth mentioning that the single point energies of **3t-opt** and **3s-opt** are close to each other. In gas phase, **3t-opt** is 1.5 kcal/mol lower in enthalpy than **3s-opt**. When taking solvation into account, the difference in enthalpy in THF is 2.1 kcal/mol. The close energy of the two species suggests that the coexistence of tetrahedral and *trans*-$[(IPr_2Me_2)_2FePh_2]$ in solution is thermodynamically permitted, which is consistent with the experimental observation of both tetrahedral and *trans*-$[(IPr_2Me_2)_2{}^{57}FePh_2]$ in solution phase. Notably, the subtle energy preference of **3t-opt** and **3s-opt** is inconsistent with the observation of *trans*-$[(IPr_2Me_2)_2{}^{57}FePh_2]$ as the major species in frozen THF by ^{57}Fe Mössbauer study. This discrepancy could be due to the intrinsic uncertainty tolerances of DFT calculations on open-shell transition-metal complexes and/or the temperature-dependence of the equilibrium between tetrahedral and *trans*-$[(IPr_2Me_2)_2FePh_2]$ in solution.

The conversion between **3t-opt** and **3s-opt** involves the change of both molecular geometry and spin states, which could be achieved via either the stepwise pathway featuring sequential dissociation of one NHC ligand, spin-change on the three coordinate species, and association of one NHC ligand (path *a* in Scheme 2), or spin-change-coupled geometry isomerization on four-coordinate iron(II) center (path *b* in Scheme 2). Calculations on the stepwise pathway (path *a*) indicated the enthalpy of 6.9 kcal/mol required for dissociation of IPr_2Me_2 from **3t-opt** to form high-spin $(IPr_2Me_2)FePh_2$ (**7-H**) in THF solution. The spin-change barrier for the conversion of **7-H** to intermediate-spin $(IPr_2Me_2)FePh_2$ (**7-I**) evaluated by the minimum energy crossing point calculation[26] is 20.6 kcal/mol. The further coordination of IPr_2Me_2 with **7-I** to produce *trans*-$(IPr_2Me_2)_2FePh_2$ (**3s-opt**) has the reaction enthalpy of −21.7 kcal/mol.

Compared to path *a*, the pathway involving the spin-change-coupled geometry isomerization on four-coordinate iron(II) center (path *b*) has a lower energy barrier. The minimum energy crossing point[26] of the $S = 1$ and $S = 2$ energy surfaces (**MECP2**) of $(IPr_2Me_2)_2FePh_2$ is 10.8 and 8.7 kcal/mol higher in energy over **3t-opt** and **3s-opt**, respectively, in THF. Moreover, the energy gap (10.8 kcal/mol) between **MECP2** and **3t-opt** is ca. 10 kcal/mol smaller than that (20.6 kcal/mol) between **MECP1** and **7-H**, indicating that the spin-change is more readily to happen for the four-coordinate species. Supporting Information, Figure S10 shows the structure of **MECP2** and Table 3 lists its key structure parameters. Its tetrahedral FeC4 core show apparent square planar distortion with the C(aryl)−Fe−C(aryl) and C(carbene)−Fe−C(carbene) angles reaching 133.94 and 140.33°, respectively. The Fe−C(aryl) distances in **MECP2** are close to those in **3s-opt**, whereas the Fe−C(carbene) separations are closer to those in **3t-opt**.

Scheme 2. Possible Pathways for the Tetrahedral-Square Planar Isomerization[a,b]

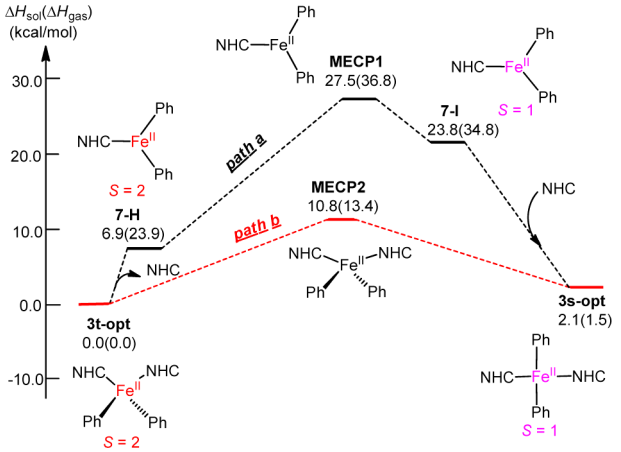

[a] $\Delta H_{sol}(\Delta H_{gas})$ is the relative enthalpy in THF solution and gas-phase, respectively. [b] NHC = IPr_2Me_2

The existence of tetrahedral−square planar isomerization is a well-recognized phenomenon for copper(II), nickel(II), and cobalt(II)[27,28] but has remained unknown for iron. In the absence of chelating enforcement, four-coordinate iron(II) complexes generally hold a tetrahedral coordination geometry. Square planar iron(II) complexes supported by monodentate ligands are rare and restricted to the bulky aryl complexes L_2FeAr_2 (L = phosphines, phosphites; Ar = C_6Cl_5, Mes),[9b] and the dimethyl complex *trans*-$[(IMes)_2FeMe_2]$.[19e] The iron(II) diaryl complexes $(IPr_2Me_2)_2FeAr_2$ reported herein, however, could exist as a mixture of tetrahedral and square planar isomers in solution phase. The geometrical preference should be the result of the intricate balance of the electronic and steric effects of the ligands. Previous studies have shown that the four-coordinate iron(II) complexes $(IPr_2Me_2)_2FeCl_2$,[17] $(IPr_2Me_2)_2FePhBr$,[18] and $[Li(Et_2O)_2][Li(1,4\text{-dioxane})][FePh_4]$[8] are high-spin tetrahedral complexes. Thus, the unique structural feature of these monodentate NHC-supported iron(II) diaryl complexes should result from the joint effect of the relative strong ligand field exerted by the four carbon-based ligands and the steric-demanding nature of NHC ligands.

CONCLUSION

In this study we have shown an NHC ligand, IPr_2Me_2, is able to stabilize a series of four-coordinate iron(II) diaryl compounds in the form of $[(IPr_2Me_2)_2FeAr_2]$ (Ar = Ph, C_6H_4-*p*-Me, C_6H_4-*p*-^{t}Bu, C_6H_3-3,5-$(CF_3)_2$) irrespective of the electron-donating or -withdrawing nature of the substituents on the aryl groups. These iron(II) diaryl compounds can be isolated as either high-spin tetrahedral structures or intermediate-spin trans square planar structures in crystalline form. Solution property studies, including solution magnetic susceptibility, absorption spectra,

DOI: 10.1021/acs.inorgchem.5b00138
Inorg. Chem. 2015, 54, 4752−4760

VT-NMR, and solution ^{57}Fe Mössbauer spectrum measurements, collectively suggest that spin-change-coupled tetrahedral−square planar equilibriums exist in the solutions of these iron(II) diaryl complexes. DFT calculations revealed the energy closeness of high-spin tetrahedral $[(IPr_2Me_2)_2FePh_2]$ and intermediate-spin *trans*-$[(IPr_2Me_2)_2FePh_2]$ and that the two species can convert to each other via spin-change coupled tetrahedral−square planar isomerization. Persistent with our goal of probing the effect of the spin-state on the reactivity of organoiron complexes, we are now designing new iron(II) diaryl complexes with fixed coordination geometry for reactivity study.

EXPERIMENTAL SECTION

General Procedures. All experiments were performed under an atmosphere of dry dinitrogen with the rigid exclusion of air and moisture using standard Schlenk or cannula techniques, or in a glovebox. All organic solvents were freshly distilled from sodium benzophenone ketyl immediately prior to use. $[(IPr_2Me_2)_2FeCl_2]$,[17] $[(IEt_2Me_2)_2Fe(CH_2TMS)_2]$,[17] *trans*-$[(IMes)_2FeMe_2]$,[19e] and ArMgBr[29] were prepared according to literature methods. All chemicals were purchased from either Strem or J&K Chemical Co. and used as received unless otherwise noted. ^{1}H and ^{19}F NMR spectra were recorded on an Agilent or Varian Mercury 300, 400, or 600 MHz spectrometer. All chemical shifts were reported in δ units with references to the residual protons of the deuterated solvents for proton chemical shifts and to ^{19}F of CF_3COOH for fluorine chemical shifts. Elemental analysis was performed by the Analytical Laboratory of Shanghai Institute of Organic Chemistry (CAS). Magnetic moments were measured at 29 °C by the method originally described by Evans with stock and experimental solutions containing a known amount of a $(CH_3)_3SiOSi(CH_3)_3$ standard.[23] Absorption spectra were recorded with a Shimadzu UV-3600 UV−vis−near-IR spectrophotometer. Magnetic measurements on crystalline samples of **5t** and **6s**·2dioxane were performed at an applied field of 2 kOe on a Quantum Design MPMP-XL7 superconducting quantum interference device (SQUID) magnetometer working in the temperature range of 300−1.8 K. The molar magnetic susceptibilities were corrected for the diamagnetism estimated from Pascal's tables and for sample holder by previous calibration. The ^{57}Fe Mössbauer spectra were measured with a constant acceleration spectrometer at 80 K. Low temperature was maintained by a CCS-850 Mössbauer Cryostat system (Janis Research Company). Data were analyzed with MossWinn 4.0Pre (Provider: Beijing Shengtianjiayuan Keji Company). Isomer shifts are relative to iron metal at room temperature.

Preparation of Tetrahedral $[(IPr_2Me_2)_2{}^{57}FePh_2]$ (3t-^{57}Fe). To a suspension of $^{57}FeCl_2$ (0.10 g, 0.78 mmol) in THF (10 mL) was added IPr_2Me_2 (0.28 g, 1.57 mmol) at room temperature. After this mixture was stirred for 10 h, dioxane (2 mL) was added to the white suspension. The resulting mixture was then cooled to −78 °C, and a THF solution of PhMgBr (1.0 M, 1.72 mL, 1.72 mmol) was added, after which the mixture warmed to room temperature. There was a color change observed gradually from light brown to yellow. After the mixture stirred for 8 h, the solvent was removed, and the residue was extracted with diethyl ether (5 mL × 3) and filtered. The filtrate was concentrated to ∼10 mL. Slow evaporation of diethyl ether afforded the diphenyl complex as a yellow crystalline solid (0.17 g, 38% yield). Dissolution of this paramagnetic complex gave a yellow solution with same ^{1}H NMR spectrum as **1** (mp 135 °C (decomp)) observed in C_6D_6. ^{1}H NMR (300 MHz, C_6D_6, 302 K): δ 60.74, −7.41.

Preparation of Tetrahedral $[(IPr_2Me_2)_2Fe(C_6H_4\text{-}p\text{-}Me)_2]$ (4t). To a suspension of $[(IPr_2Me_2)_2FeCl_2]$ (0.30 g, 0.65 mmol) in THF/dioxane (10 mL/2 mL) was added a THF solution of *p*-Me-C_6H_4MgBr, prepared from the interaction of *p*-Me-C_6H_4Br (0.28 g, 1.63 mmol) with magnesium (0.078 g, 3.26 mmol) in THF, at −78 °C. The resulting mixture was warmed to room temperature. There was a gradual color change observed from light brown to yellow. After the mixture stirred for 8 h, the solvent was removed, and the residue was extracted with diethyl ether (5 mL × 3) and filtered. The filtrate was concentrated to ∼10 mL. Slow evaporation of diethyl ether afforded the product as a yellow crystalline solid (0.20 g, 50% yield). Anal. Calcd for $C_{36}H_{54}FeN_4$: C, 72.22; H, 9.09; N, 9.36. Found: C, 71.88; H, 8.95; N, 9.51%. UV−vis−NIR absorption: λ_{max}(benzene)/nm 340 (ε/dm^3 mol^{-1} cm^{-1} 2950), 1352 (120) and 1500 (170). The ^{1}H NMR spectrum of **4t** displayed three characteristic peaks in the range from +150 to −150 ppm in C_6D_6. ^{1}H NMR (300 MHz, C_6D_6, 302 K): δ 65.81, 62.91, −1.19. Magnetic susceptibility (C_6D_6, 302 K): μ_{eff} = 4.4(1) μ_B.

Preparation of Tetrahedral $[(IPr_2Me_2)_2Fe(C_6H_4\text{-}p\text{-}{}^tBu)_2]$ (5t). To a suspension of $[(IPr_2Me_2)_2FeCl_2]$ (0.30 g, 0.65 mmol) in THF/dioxane (10 mL/2 mL) was added a THF solution of *p*-^{t}Bu-C_6H_4MgBr, prepared from the interaction of *p*-^{t}Bu-C_6H_4Br (0.35 g, 1.63 mmol) with magnesium (0.078 g, 3.26 mmol) in THF, at −78 °C. The resulting mixture was warmed to room temperature. There was a gradual color change observed from light brown to yellow. After the mixture stirred for 8 h, the solvent was removed, and the residue was extracted with diethyl ether (5 mL × 3) and filtered. The filtrate was concentrated to ∼10 mL. Slow evaporation of diethyl ether afforded the product as a yellow, crystalline solid (0.24 g, 53% yield). Anal. Calcd for $C_{42}H_{66}FeN_4$: C, 73.87; H, 9.74; N, 8.20. Found: C, 73.45; H, 9.77; N, 7.93%. UV−vis−NIR absorption: λ_{max}(benzene)/nm 340 (ε/dm^3 mol^{-1} cm^{-1} 2540), 1350 (140) and 1500 (160). The ^{1}H NMR spectrum of **5t** displayed three characteristic peaks in the range from +150 to −150 ppm in C_6D_6. ^{1}H NMR (300 MHz, C_6D_6, 302 K): δ 62.25, 17.32, −6.20. Magnetic susceptibility (C_6D_6, 302 K): μ_{eff} = 4.1(2) μ_B. mp 126 °C (decomp).

Preparation of trans-$[(IPr_2Me_2)_2Fe(C_6H_3\text{-}3,5\text{-}(CF_3)_2)_2]$ (6s). To a suspension of $[(IPr_2Me_2)_2FeCl_2]$ (0.30 g, 0.65 mmol) in THF/dioxane (10 mL/2 mL) was added a THF solution of 3,5-$(CF_3)_2$-C_6H_3MgBr, prepared from the interaction of 3,5-$(CF_3)_2$-C_6H_3Br (0.48 g, 1.63 mmol) with magnesium (0.078 g, 3.26 mmol) in THF, at −78 °C. When warmed to room temperature, the deep yellow suspension had a color change to orange. After the mixture stirred for 8 h, the solvent was removed, and the residue was extracted with diethyl ether (5 mL × 3) and filtered. The filtrate was concentrated to ∼10 mL. Slow evaporation of diethyl ether afforded the diaryl complex as a mixture of yellow and orange crystalline solid with the former being small amount. Single-crystal X-ray diffraction studies established the yellow and orange crystals are tetrahedral $[(IPr_2Me_2)_2Fe(C_6H_3\text{-}3,5\text{-}(CF_3)_2)_2]$ (**6t**) and square planar *trans*-$[(IPr_2Me_2)_2Fe(C_6H_3\text{-}3,5\text{-}(CF_3)_2)_2]$·2dioxane (**6s**·$2C_4H_8O_2$), respectively. Combined yield: 0.28 g, 52%. Anal. Calcd for $C_{38}H_{46}F_{12}FeN_4$: C, 54.16; H, 5.50; N, 6.65. Found: C, 53.92; H, 5.38; N, 6.92%. UV−vis−NIR absorption: λ_{max}(benzene)/nm 330 (ε/dm^3 mol^{-1} cm^{-1} 3900), 400 (1900), 1320 (134) and 1420 (180). The ^{1}H NMR spectra of the two isomers are found identical in C_6D_6 with two very broad peaks in the range from +150 to −150 ppm in C_6D_6. ^{1}H NMR (400 MHz, C_6D_6, 304 K): δ −8.33, −10.83. ^{19}F NMR (376 MHz, C_6D_6, 304 K): δ 45.55. Magnetic susceptibility (C_6D_6, 302 K): μ_{eff} = 4.4(1) μ_B. mp for **6s**: 134 °C (decomp).

X-ray Structure Determination. All single crystals were immersed in Paraton-N oil and sealed under N_2 in thin-walled glass capillaries. Data were collected at 133 or 140 K on a Bruker AXSD8 X-ray diffractometer using Mo Kα radiation. An empirical absorption correction was applied using the SADABS program.[30] All structures were solved by direct methods, and subsequent Fourier difference techniques and were refined anisotropically for all non-hydrogen atoms by full-matrix least-squares calculations on F^2 using the SHELXTL program package.[31] All hydrogen atoms were geometrically fixed using the riding model. Crystal data and details of data collection and structure refinements for **4t**, **5t**, **6t**, and **6s**·2 $C_4H_8O_2$ are given in Supporting Information, Table S1.

Computational Details. The calculations of electronic structures and energy profile were performed with Gaussian 09 program.[24] The B3LYP density functional[25] in combination with the double-ζ valence basis set SVP[32] was used for geometry optimizations and subsequent analytic frequency calculation. Each optimized structure was characterized as a minimum (N_{Imag} = 0) or a transition state (N_{Imag}

DOI: 10.1021/acs.inorgchem.5b00138
Inorg. Chem. 2015, 54, 4752−4760

= 1). To obtain more reliable relative energies, the effect of THF solvation was considered by CPCM model with UFF atomic radii.[33] The energies in THF solution were obtained from the SCRF single-point calculations, and the gas-phase enthalpy and free energy corrections were included, respectively. In such single-point calculations, the B3LYP functional and larger basis set TZVP[34] for all atoms were utilized. The minimum energy crossing point calculation was performed by MECP program.[26] The open-shell species were treated with unrestricted manner, and the stabilities of the wave functions were tested. The symmetry of spatial orbitals was allowed to be completely broken (broken-symmetry) in search for ground state. Since the free energies were computationally over-estimated due to entropy contribution when we deal with one-to-two and two-to-one (bimolecular) transformations, the reaction enthalpies were utilized to describe the energy profiles in the text. However, the free energies of the optimized structures involved in Scheme 2 are also given in Table S2 in Supporting Information for estimation of entropy contributions in the current system.

■ ASSOCIATED CONTENT

Supporting Information

X-ray crystallographic files in CIF format; tabulated crystal data; NMR, absorption, and Mössbauer spectra of the complexes; computed relative free energies; Mulliken spin-density plots; structure of **MECP2**; and optimized coordinates by computational studies. This material is available free of charge via the Internet at http://pubs.acs.org.

■ AUTHOR INFORMATION

Corresponding Authors

*E-mail: deng@sioc.ac.cn. (L. D.)
*E-mail: luoyi@dlut.edu.cn. (Y. L.)

Author Contributions

[§]These authors contributed equally.

Notes

The authors declare no competing financial interest.

■ ACKNOWLEDGMENTS

We thank Prof. M. L. Neidig at Univ. Rochester for his generosity of providing a sample of $^{57}FeCl_2$ and helpful discussion. This research was financially supported by the Chinese Academy of Sciences, the National Basic Research Program of China (973 Program, No. 2011CB808705), the National Natural Science Foundation of China (Nos. 21222208, 21432001, 21421091, and 21429201), and the Fundamental Research Funds for the Central Universities (DUT13ZD103). The authors also thank the Network and Information Center of Dalian Univ. Technology for part of computational resources.

■ REFERENCES

(1) (a) *Iron Catalysis in Organic Chemistry: Reaction and Application;* Plietker, B., Ed.; Wiley-VCH: Weinheim, Germany, 2008. (b) Bolm, C.; Legros, J.; Paih, J. L.; Zani, L. *Chem. Rev.* **2004**, *104*, 6217. (c) Sherry, B. D.; Fürstner, A. *Acc. Chem. Res.* **2008**, *41*, 1500. (d) Czaplik, W. M.; Mayer, M.; Cvengroš, J.; Jacobi von Wangelin, A. *ChemSusChem* **2009**, *2*, 396.

(2) For recent examples, see: (a) Hatakeyama, T.; Hashimoto, S.; Ishizuka, K.; Nakamura, M. *J. Am. Chem. Soc.* **2009**, *131*, 11949. (b) Adams, C. J.; Bedford, R. B.; Carter, E.; Gower, N. J.; Haddow, M. F.; Harvey, J. N.; Huwe, M.; Cartes, M. A.; Mansell, S. M.; Mendoza, C.; Murphy, D. M.; Neeve, E. C.; Nunn, J. *J. Am. Chem. Soc.* **2012**, *134*, 10333. (c) Gülak, S.; Jacobi von Wangelin, A. *Angew. Chem., Int. Ed.* **2012**, *51*, 1357.

(3) For recent examples, see: (a) Fürstner, A.; Méndez, M. *Angew. Chem., Int. Ed.* **2003**, *42*, 5355. (b) Yamagami, T.; Shintani, R.; Shirakawa, E.; Hayashi, T. *Org. Lett.* **2007**, *9*, 1045. (c) Ito, S.; Itoh, T.; Nakamura, M. *Angew. Chem., Int. Ed.* **2011**, *50*, 454.

(4) For recent examples, see: (a) Norinder, J.; Matsumoto, A.; Yoshikai, N.; Nakamura, E. *J. Am. Chem. Soc.* **2008**, *130*, 5858. (b) Ilies, L.; Asako, S.; Nakamura, E. *J. Am. Chem. Soc.* **2011**, *133*, 7672. (c) Shang, R.; Ilies, L.; Matsumoto, A.; Nakamura, E. *J. Am. Chem. Soc.* **2013**, *135*, 6030. (d) Matsubara, T.; Asako, S.; Ilies, L.; Nakamura, E. *J. Am. Chem. Soc.* **2014**, *136*, 646.

(5) For reviews on open-shell organometallic chemistry, please see: (a) Poli, R. *Chem. Rev.* **1996**, *96*, 2135. (b) Schröder, D.; Shaik, S.; Schwarz, H. *Acc. Chem. Res.* **2000**, *33*, 139. (c) Poli, R.; Harvey, J. N. *Chem. Soc. Rev.* **2003**, *32*, 1.

(6) Rangheard, C.; de Julián Fernández, C.; Phua, P.-H.; Hoorn, J.; Lefort, L.; de Vries, J. G. *Dalton Trans.* **2010**, *39*, 8464.

(7) Klose, A.; Solari, E.; Floriani, C.; Chiesi-Villa, A.; Rizzoli, C.; Re, N. *J. Am. Chem. Soc.* **1994**, *116*, 9123.

(8) Fürstner, A.; Martin, R.; Krause, H.; Seidel, G.; Goddard, R.; Lehmann, C. W. *J. Am. Chem. Soc.* **2008**, *130*, 8773.

(9) For examples, see: (a) Chatt, J.; Shaw, B. L. *J. Chem. Soc.* **1961**, 285. (b) Hawrelak, E. J.; Bernskoetter, W. H.; Lobkovsky, E.; Yee, G. T.; Bill, E.; Chirik, P. J. *Inorg. Chem.* **2005**, *44*, 3103. (c) Alonso, P. J.; Arauzo, A. B.; Forniés, J.; García-Monforte, M. A.; Martín, A.; Martínez, J. I.; Menjón, B.; Rillo, C.; Sáiz-Garitaonandia, J. J. *Angew. Chem., Int. Ed.* **2006**, *45*, 6707. (d) Wunderlich, S. H.; Knochel, P. *Angew. Chem., Int. Ed.* **2009**, *48*, 9717. (e) Volbeda, J.; Meetsma, A.; Bouwkamp, M. W. *Organometallics* **2009**, *28*, 209.

(10) For examples, see: (a) Wehmschulte, R. J.; Power, P. P. *Organometallics* **1995**, *14*, 3264. (b) Müller, H.; Seidel, W.; Görls, H. *Angew. Chem., Int. Ed.* **1995**, *34*, 325. (c) Sutton, A. D.; Ngyuen, T.; Fettinger, J. C.; Olmstead, M. M.; Long, G. J.; Power, P. P. *Inorg. Chem.* **2007**, *46*, 4809. (d) Kays, D. L.; Cowley, A. R. *Chem. Commun.* **2007**, 1053. (e) Ni, C.; Ellis, B. D.; Fettinger, J. C.; Long, G. J.; Power, P. P. *Chem. Commun.* **2008**, 1014. (f) Ni, C.; Fettinger, J. C.; Long, G. J.; Power, P. P. *Inorg. Chem.* **2009**, *48*, 2443. (g) Noda, D.; Sunada, Y.; Hatakeyama, T.; Nakamura, M.; Nagashima, H. *J. Am. Chem. Soc.* **2009**, *131*, 6078. (h) Lei, H.; Guo, J.-D.; Fettinger, J. C.; Nagase, S.; Power, P. P. *J. Am. Chem. Soc.* **2010**, *132*, 17399. (i) Weismann, D.; Sun, Y.; Lan, Y.; Wolmershäuser, G.; Powell, A. K.; Sitzmann, H. *Chem.—Eur. J.* **2011**, *17*, 4700. (j) Daifuku, S. L.; Al-Afyouni, M. H.; Snyder, B. E. R.; Kneebone, J. L.; Neidig, M. L. *J. Am. Chem. Soc.* **2014**, *136*, 9132.

(11) For recent reviews covering iron complexes of sterically demanding aryls, see: (a) Power, P. P. *Chem. Rev.* **2012**, *112*, 3482. (b) Kays, D. L. *Dalton Trans.* **2011**, *40*, 769.

(12) Wingerter, S.; Pfeiffer, M.; Stey, T.; Bolboacá, M.; Kiefer, W.; Chandrasekhar, V.; Stalke, D. *Organometallics* **2001**, *20*, 2730.

(13) (a) Yu, Y.; Brennessel, W. W.; Holland, P. L. *Organometallics* **2007**, *26*, 3217. (b) Fernández, I.; Trovitch, R. J.; Lobkovsky, E.; Chirik, P. J. *Organometallics* **2008**, *27*, 109. (c) Ohki, Y.; Hatanaka, T.; Tatsumi, K. *J. Am. Chem. Soc.* **2008**, *130*, 17174. (d) Hatanaka, T.; Ohki, Y.; Tatsumi, K. *Chem.—Asian J.* **2010**, *5*, 1657. (e) Jové, F. A.; Pariya, C.; Scoblete, M.; Yap, G. P. A.; Theopold, K. H. *Chem.—Eur. J.* **2011**, *17*, 1310.

(14) For examples, see: (a) Bedford, R. B.; Betham, M.; Bruce, D. W.; Danopoulos, A. A.; Frost, R. M.; Hird, M. *J. Org. Chem.* **2006**, *71*, 1104. (b) Ghorai, S. K.; Jin, M.; Hatakeyama, T.; Nakamura, M. *Org. Lett.* **2012**, *14*, 1066. (c) Gao, H.-H.; Yan, C.-H.; Tao, X.-P.; Xia, Y.; Sun, H.-M.; Shen, Q.; Zhang, Y. *Organometallics* **2010**, *29*, 4189. The recent reviews: (d) Ingleson, M. J.; Layfield, R. A. *Chem. Commun.* **2012**, *48*, 3579. (e) Bézier, D.; Sortais, J.-B.; Darcel, C. *Adv. Synth. Catal.* **2013**, *355*, 19.

(15) Liu, Y.; Shi, M.; Deng, L. *Organometallics* **2014**, *33*, 5660.

(16) (a) Przyojski, J. A.; Arman, H. D.; Tonzetich, Z. J. *Organometallics* **2012**, *31*, 3264. (b) Danopoulos, A. A.; Braunstein, P.; Wesolek, M.; Monakhov, K. Y.; Rabu, P.; Robert, V. *Organometallics* **2012**, *31*, 4102.

(17) Xiang, L.; Xiao, J.; Deng, L. *Organometallics* **2011**, *30*, 2018.

DOI: 10.1021/acs.inorgchem.5b00138
Inorg. Chem. 2015, 54, 4752−4760

(18) Liu, Y.; Xiao, J.; Wang, L.; Song, Y.; Deng, L. *Organometallics* **2015**, *34*, 599.
(19) (a) Zlatogorsky, S.; Muryn, C. A.; Tuna, F.; Evans, D. J.; Ingleson, M. J. *Organometallics* **2011**, *30*, 4974. (b) Danopoulos, A. A.; Braunstein, P.; Stylianides, N.; Wesolek, M. *Organometallics* **2011**, *30*, 6514. (c) Meyer, S.; Orben, C. M.; Demeshko, S.; Dechert, S.; Meyer, F. *Organometallics* **2011**, *30*, 6692. (d) Layfield, R. A.; McDouall, J. J. W.; Scheer, M.; Schwarzmaier, C.; Tuna, F. *Chem. Commun.* **2011**, *47*, 10623. (e) Hashimoto, T.; Urban, S.; Hoshino, R.; Ohki, Y.; Tatsumi, K.; Glorius, F. *Organometallics* **2012**, *31*, 4474. (f) Wang, X.; Mo, Z.; Xiao, J.; Deng, L. *Inorg. Chem.* **2013**, *52*, 59. (g) Danopoulos, A. A.; Monakhov, K. Y.; Braunstein, P. *Chem.—Eur. J.* **2013**, *19*, 450. (h) Day, B. M.; Pugh, T.; Hendriks, D.; Guerra, C. F.; Evans, D. J.; Bickelhaupt, F. M.; Layfield, R. A. *J. Am. Chem. Soc.* **2013**, *135*, 13338.
(20) Semproni, S. P.; Milsmann, C.; Chirik, P. J. *J. Am. Chem. Soc.* **2014**, *136*, 9211.
(21) Muller, G.; Sales, J.; Vinaixa, J.; Tejada, J. *Inorg. Chim. Acta* **1982**, *60*, 227.
(22) Fillman, K. L.; Przyojski, J. A.; Al-Afyouni, M. H.; Tonzetich, Z. J.; Neidig, M. L. *Chem. Sci.* **2015**, *6*, 1178.
(23) (a) Evans, D. F. *J. Chem. Soc.* **1959**, 2003. (b) Sur, S. K. *J. Magn. Reson.* **1989**, *82*, 169.
(24) Frisch, M. J.; Trucks, G. W.; Schlegel, H. B.; Scuseria, G. E.; Robb, M. A.; Cheeseman, J. R.; Scalmani, G.; Barone, V.; Mennucci, B.; Petersson, G. A.; Nakatsuji, H.; Caricato, M.; Li, X.; Hratchian, H. P.; Izmaylov, A. F.; Bloino, J.; Zheng, G.; Sonnenberg, J. L.; Hada, M.; Ehara, M.; Toyota, K.; Fukuda, R.; Hasegawa, J.; Ishida, M.; Nakajima, T.; Honda, Y.; Kitao, O.; Nakai, H.; Vreven, T.; Montgomery, J. A., Jr.; Peralta, J. E.; Ogliaro, F.; Bearpark, M.; Heyd, J. J.; Brothers, E.; Kudin, K. N.; Staroverov, V. N.; Kobayashi, R.; Normand, J.; Raghavachari, K.; Rendell, A.; Burant, J. C.; Iyengar, S. S.; Tomasi, J.; Cossi, M.; Rega, N.; Millam, N. J.; Klene, M.; Knox, J. E.; Cross, J. B.; Bakken, V.; Adamo, C.; Jaramillo, J.; Gomperts, R.; Stratmann, R. E.; Yazyev, O.; Austin, A. J.; Cammi, R.; Pomelli, C.; Ochterski, J. W.; Martin, R. L.; Morokuma, K.; Zakrzewski, V. G.; Voth, G. A.; Salvador, P.; Dannenberg, J. J.; Dapprich, S.; Daniels, A. D.; Farkas, Ö.; Foresman, J. B.; Ortiz, J. V.; Cioslowski, J.; Fox, D. J. *Gaussian 09*, Revision A.02; Gaussian, Inc.: Wallingford, CT, 2009.
(25) (a) Becke, A. D. *J. Chem. Phys.* **1993**, *98*, 5648. (b) Lee, C.; Yang, W.; Parr, R. G. *Phys. Rev. B* **1988**, *37*, 785.
(26) Minimum energy crossing points (MECP) were calculated using the MECP program of Harvey et al.; see Harvey, J. N.; Aschi, M.; Schwarz, H.; Koch, W. *Theor. Chem. Acc.* **1998**, *99*, 95.
(27) Ingleson, M. J.; Pink, M.; Fan, H.; Caulton, K. G. *Inorg. Chem.* **2007**, *46*, 10321.
(28) For examples, see: (a) Gaăzo, J.; Bersuker, I. B.; Garaj, J.; Kabešová, M.; Kohout, J.; Langfelderová, H.; Melník, M.; Serator, M.; Valach, F. *Coord. Chem. Rev.* **1976**, *19*, 253. (b) Holm, R. H.; Chakravorty, A.; Theriot, L. J. *Inorg. Chem.* **1966**, *5*, 625. (c) Wolny, J. A.; Rudolf, M. F.; Ciunik, Z.; Gatner, K.; Wolowiec, S. *J. Chem. Soc., Dalton Trans.* **1993**, 1611.
(29) Anbarasan, P.; Neumann, H.; Beller, M. *Chem.—Eur. J.* **2010**, *16*, 4725.
(30) Sheldrick, G. M. *SADABS*, Program for Empirical Absorption Correction of Area Detector Data; University of Göttingen: Germany, 1996.
(31) Sheldrick, G. M. *SHELXTL*, Version 5.10 for Windows NT: Structure Determination Software Programs; Bruker Analytical X-ray systems, Inc.: Madison, WI, 1997.
(32) Schäfer, A.; Horn, H.; Ahlrichs, R. *J. Chem. Phys.* **1992**, *97*, 2571.
(33) (a) Miertuš, S.; Scrocco, E.; Tomasi, J. *Chem. Phys.* **1981**, *55*, 117. (b) Cammi, R.; Mennucci, B.; Tomasi, J. *J. Phys. Chem. A* **2000**, *104*, 5631.
(34) Schäfer, A.; Huber, C.; Ahlrichs, R. *J. Chem. Phys.* **1994**, *100*, 5829.

DOI: 10.1021/acs.inorgchem.5b00138
Inorg. Chem. 2015, 54, 4752−4760